Exploiting the S4–S5 Specificity of Human Neutrophil Proteinase 3 to Improve the Potency of Peptidyl Di(chlorophenyl)-phosphonate Ester Inhibitors: A Kinetic and Molecular Modeling Analysis

Carla Guarino, Natalia Gruba, Renata Grzywa, Edyta Dyguda-Kazimierowicz, Yveline Hamon, Monika Ł gowska, Marcin Skoreński, Sandrine Dallet-Choisy, Adam Marchand-Adam, Christine Kellenberger, et al.

HAL Id: hal-02094546
https://amu.hal.science/hal-02094546

Submitted on 9 Apr 2019

Exploiting the S4–S5 Specificity of Human Neutrophil Proteinase 3 to Improve the Potency of Peptidyl Di(chlorophenyl)-phosphonate Ester Inhibitors: A Kinetic and Molecular Modeling Analysis

Carla Guarino, Natalia Gruba, Renata Grzywa, Edyta Dyguda-Kazimierowicz, Yveline Hamon, Monika Ł gowska, Marcin Skoreński, Sandrine Dallet-Choisy, Adam Marchand-Adam, Christine Kellenberger, et al.

HAL Id: hal-02094546

https://hal-amu.archives-ouvertes.fr/hal-02094546

Submitted on 9 Apr 2019

Exploiting the S4−S5 Specificity of Human Neutrophil Proteinase 3 to Improve the Potency of Peptidyl Di(chlorophenyl)-phosphonate Ester Inhibitors: A Kinetic and Molecular Modeling Analysis

Carla Guarino,[†] Natalia Gruba,[‡] Renata Grzywa,[§] Edyta Dyguda-Kazimierowicz,[‖] Yveline Hamon,[†]
Monika Legowska,[‡] Marcin Skoreński,[§] Sandrine Dallet-Choisy,[†] Sylvain Marchand-Adam,[†]
Christine Kellenberger,[⊥] Dieter E. Jenne,[#] Marcin Sienczyk,[§] Adam Lesner,[‡] Francis Gauthier,[†]
and Brice Korkmaz*,[†]

[†]INSERM U-1100, "Centre d'Etude des Pathologies Respiratoires", Université François Rabelais, 37032 Tours, France

[‡]Faculty of Chemistry, University of Gdansk, Wita Stwosza 63, 80-308 Gdansk, Poland
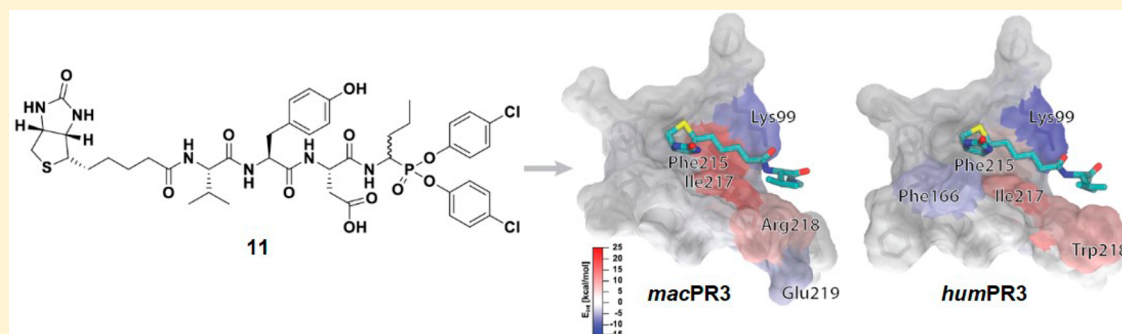
[§]Faculty of Chemistry, Division of Medicinal Chemistry and Microbiology, Wroclaw University of Science and Technology, Wyb. Wyspianskiego 27, 50-370 Wroclaw, Poland

[‖]Faculty of Chemistry, Advanced Materials Engineering and Modelling Group, Wroclaw University of Science and Technology, Wyb. Wyspianskiego 27, 50-370 Wroclaw, Poland

[⊥]Architecture et Fonction des Macromolécules Biologiques, CNRS-Unité Mixte de Recherche (UMR), 13288 Marseille, France

[#]Institute of Lung Biology and Disease, German Center for Lung Research (DZL), Comprehensive Pneumology Center Munich and Max Planck Institute of Neurobiology, 82152 Planegg-Martinsried, Germany
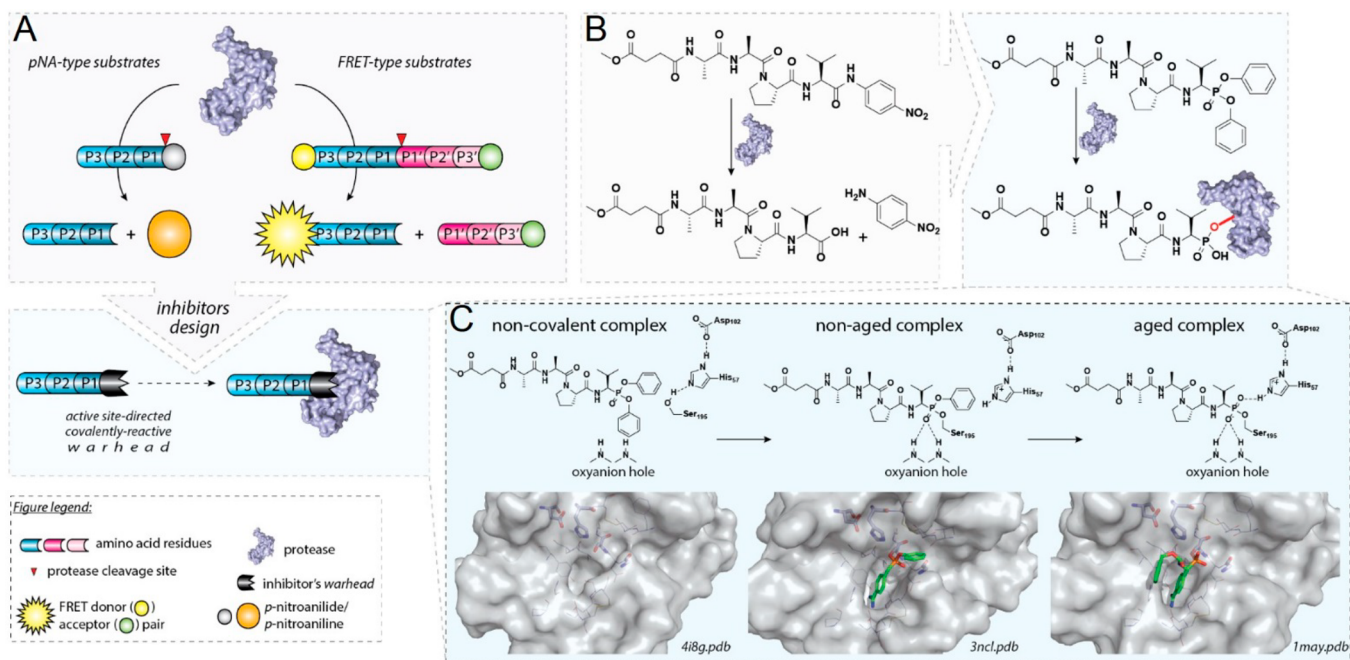
S *Supporting Information*

ABSTRACT: The neutrophilic serine protease proteinase 3 (PR3) is involved in inflammation and immune response and thus appears as a therapeutic target for a variety of infectious and inflammatory diseases. Here we combined kinetic and molecular docking studies to increase the potency of peptidyl-diphenyl phosphonate PR3 inhibitors. Occupancy of the S1 subsite of PR3 by a nVal residue and of the S4−S5 subsites by a biotinylated Val residue as obtained in biotin-VYDnV$^\text{P}$(O-C$_6$H$_4$-4-Cl)$_2$ enhanced the second-order inhibition constant $k_\text{obs}/[\text{I}]$ toward PR3 by more than 10 times ($k_\text{obs}/[\text{I}] = 73000 \pm 5000$ M^{-1} s^{-1}) as compared to the best phosphonate PR3 inhibitor previously reported. This inhibitor shows no significant inhibitory activity toward human neutrophil elastase and resists proteolytic degradation in sputa from cystic fibrosis patients. It also inhibits macaque PR3 but not the PR3 from rodents and can thus be used for in vivo assays in a primate model of inflammation.

■ INTRODUCTION

Polymorphonuclear neutrophil phagocytes are characterized by the presence of abundant intracytoplasmic granules rich in antimicrobial peptides and proteins involved in innate immunity.[1,2] Azurophilic granules also store four neutrophil serine proteases (NSPs): proteinase 3 (PR3), elastase (NE), cathepsin G (CG), and neutrophil serine protease 4 (NSP-4), which are released into the environment in response to inflammatory stimuli.[1,3] An excess of proteases may be released, however, during chronic inflammation which disrupts the protease−protease inhibitor balance and accelerates proteolysis of the extracellular matrix.[4,5] The administration of exogenous inhibitors targeting these proteases may thus be an excellent therapeutic strategy to fight inflammation.[5,6] Although the total amount of PR3 in neutrophils is similar to that of NE or CG, its activity is by far less controlled by endogenous inhibitors.[7] Indeed, there is no specific endogenous inhibitor of human PR3 (humPR3) and one of its more potent inhibitors, α-1-proteinase inhibitor (α1PI), interacts about 100 times less

Figure 1. Design, structure, and mechanism of action of 1-aminoalkylphosphonate diaryl ester inhibitors. (A) General strategy of a substrate-based approach for covalent inhibitors development. (B) Development of a peptidyl-phosphonate inhibitor. (C) Mechanism of serine proteases inhibition by 1-aminoalkylphosphonate diaryl esters together with crystal structures of bovine trypsin (Protein Data Bank (PDB) 4I8G and 1MAY) and human matriptase (PDB 3NCL) at different stages of aging process.

rapidly with *hum*PR3 than with *hum*NE.[7] Further, the pathophysiological role of *hum*PR3 is less well understood than that of the related *hum*NE and CG. Its function as autoantigen in granulomatosis with polyangiitis[8−10] and its likely involvement in neutrophil apoptosis[11] makes it different from its closest homologue *hum*NE.

*hum*PR3 closely resembles *hum*NE structurally and functionally with a highly conserved catalytic triad (His57, Asp102, and Ser195 residues (*chymotrypsinogen numbering*)) located between two similar domains each comprising a six-stranded β-barrel.[12] Its p*I*, however, is somewhat less basic than that of *hum*NE.[5,13] Several residues on the loops surrounding the protease active site assist the catalytic process. Most importantly, the backbone amide hydrogens of Gly193 and Ser195 that define the oxyanion hole and are located near the carbonyl group of the substrate's scissile bond, stabilizing the developing partial charge on the tetrahedral intermediate during catalysis.[14]

The structural analysis of the active site of *hum*PR3 and *hum*NE showed that the distribution of charged residues close to the substrate binding site (99 loop, 60 loop, 37 loop, and autolysis loop) of these two proteases differs notably.[15] Thus, *hum*PR3 contains three charged residues Lys99, Asp61, and Arg143 in the active site region.[12] The S1 binding pocket of *hum*PR3 and *hum*NE is hemispherical, therefore, both preferentially accommodate small hydrophobic residues at the P1 position (according to the nomenclature of Schechter and Berger (Schechter and Berger, 1967)).[7,13] The S2 subsite of *hum*PR3 differs from that of *hum*NE by the presence of a solvent accessible Lys at position 99, favoring accommodation of negatively charged or polar P2 residues in the deep S2 subsite of PR3.[12] The Leu99 residue in *hum*NE makes the S2 pocket more hydrophobic. The Lys99 of *hum*PR3 is conserved in the PR3 of higher primates and many artiodactyls but not in PR3 of New World monkeys and rodents, whereas the Leu99

of *hum*NE is highly conserved in many other species.[7] This makes the PR3 specificity of these latter species different from that of *hum*PR3 and explains that rodents are not an appropriate animal model for studies related to the biological activity of *hum*PR3. Another critical residue that makes the specificities of *hum*PR3 and *hum*NE different is that at position 217 in the vicinity of the S4 subsite, where an Ile in *hum*PR3 is replaced by an Arg in *hum*NE.[16,17]

We have designed and synthesized selective peptidyl-diphenyl phosphonate inhibitors based on these structural differences between *hum*PR3 and *hum*NE using the sequence of an optimized peptide substrate of PR3.[18] Phosphonate inhibitors are peptide-based transition state irreversible inhibitors which form transition-state-resembling complexes with serine proteases.[19−21] The inhibition is initiated by the formation of a noncovalent enzyme–inhibitor complex, which upon the nucleophilic attack of the Ser195 on the phosphorus atom loses one aryloxy group, forming an initial, irreversible covalent complex (Figure 1). Further aging followed by hydrolysis of a second ester group leads to the formation of an aged covalent protease–inhibitor complex stabilized by the oxyanion hole.[19] Phosphonate inhibitors are chemically stable inhibitors that block selectively serine proteases at low concentration under acidic or neutral conditions.[22] Phosphonate inhibitors were designed and developed by anchoring of the serine trap to the recognition sequence derived from a peptidyl substrate of the target protease (Figure 1). These inhibitors which interact covalently with the Ser195 of the catalytic triad can also be used as activity-based probes (ABP)[23] to visualize membrane-bound or intracellular, proteolytically active, serine proteases.[24] Several peptidyl-diphenyl phosphonate inhibitors of *hum*PR3 have been developed but all were more potent toward *hum*NE[25,26] until we synthesized the first selective chlorodiphenyl phosphonate *hum*PR3 inhibitors, the

Table 1. Rates of Inhibition of *hum*PR3 and *hum*NE by Peptide Phosphonates

			proteases	
			$k_{obs}/[I]$ $(M^{-1}\ s^{-1})^a$	
compd	peptide phosphonate esters	$[I]\ \mu M$	*hum*PR3	*hum*NE
1	Ac-Pro-Tyr-Asp-AlaP(O-C$_6$H$_4$-4-Cl)$_2$	2	154 ± 3^b	ns
2	Bt-Pro-Tyr-Asp-AlaP(O-C$_6$H$_4$-4-Cl)$_2$	0.06	$4168 \pm 553^{\#}$	ns
3	Bt-[**PEG**]**2**-Pro-Tyr-Asp-AlaP(O-C$_6$H$_4$-4-Cl)$_2$	0.6	274 ± 12	ns
4	Bt-**Val**-Tyr-Asp-AlaP(O-C$_6$H$_4$-4-Cl)$_2$	0.025	17396 ± 835	ns
5	Bt-**Leu**-Tyr-Asp-AlaP(O-C$_6$H$_4$4-Cl)$_2$	0.15	4371 ± 652	ns
6	Bt-**Ile**-Tyr-Asp-AlaP(O-C$_6$H$_4$-4-Cl)$_2$	0.15	8698 ± 658	ns
7	Bt-**nLeu**-Tyr-Asp-AlaP(O-C$_6$H$_4$-4-Cl)$_2$	0.025	10361 ± 766	ns
8	Bt-**nLeu**(*O*-**Bzl**)-Tyr-Asp-AlaP(O-C$_6$H$_4$-4-Cl)$_2$	0.1	1744 ± 164	ns
9	Bt-Pro-Tyr-Asp-**Abu**P (O-C$_6$H$_4$-4-Cl)$_2$	0.1	4675 ± 438	ns
10	Bt-Pro-Tyr-Asp-**nVal**P(O-C$_6$H$_4$-4-Cl)$_2$	0.025	18642 ± 705	ns
11	Bt-**Val**-Tyr-Asp-**nVal**P(O-C$_6$H$_4$-4-Cl)$_2$	0.01	73258 ± 5342	ns

^{a}Values are the means $\pm$ SD of three experiments; ^{b}Values were taken from ref 18. Definition of abbreviation: ns, not significant

N-biotinylation of which allows using them ABP to visualize active *hum*PR3 in biological samples.[18]

Application of PR3 inhibitors as therapeutic tools requires that they easily reach and interact with their target protease with great specificity, they resist degradation during their administration and in situ, and their half-life in the organism is significant. Using inhibitors as therapeutic tools also requires that a relevant animal model is available for preclinical studies. In this work, we first designed and developed new biotin-peptidyl^P(O-C$_6$H$_4$-4-Cl)$_2$ inhibitors with improved potency of action toward *hum*PR3 to use them as versatile pharmacological tools for assessing protease function in vivo. We focused on improving the rate constant for inactivation ($k_{obs}/[I]$) by molecular docking trials and on analyzing structure−activity relationships (SAR) to optimize efficacy at a very low dose and thus make the resulting compound effective for a pharmacological application. Because PR3 from rodents retain a substrate specificity that differs from that of human,[27] we then looked for a relevant in vivo model of inflammation and tested phosphonate inhibitors on the PR3 from *Macaca fascicularis*.

■ RESULTS

Stabilizing Properties of a Biotinylated N-Terminal P4 Residue in PR3 Substrates and Inhibitors. Replacing the N-terminal acetyl group by biotin (Bt) in Ac-PYDA^P(O-C$_6$H$_4$-4-Cl)$_2$ (**1**) to give Bt-PYDA^P(O-C$_6$H$_4$-4-Cl)$_2$ (**2**) significantly improved the $k_{obs}/[I]$ value[18] ($4168\ M^{-1}\ s^{-1}$ vs $154\ M^{-1}\ s^{-1}$) (Table 1) and significantly improved the K_i value of the initial noncovalent complex (21 vs 3600 nM) (Table 2). Accordingly, the substitution of the N-terminal acetyl group by a biotin in the paranitroanilide (pNA) substrate Ac-PYDA-pNA increased the specificity constant k_{cat}/K_m by ∼6-fold (Table 3). We employed a computational docking approach to explain how biotin could modulate the interaction between Bt-PYDA^P(O-C$_6$H$_4$-Cl)$_2$ and the active site of PR3 (Figure 2A,B). The lowest energy binding mode obtained in the docking studies of **2** with *hum*PR3 revealed that the biotin moiety is located in the S5 pocket limited by the Lys99, Phe166, Cys168, Arg177, and Ile217 residues (Figure 2B). The entrance into this pocket is guarded by the Lys99 side chain with its ε-amino group, creating a hydrogen bonding with the carbonyl oxygen of the Bt-Pro4 amide bond. This interaction would facilitate the correct orientation of both Pro4 and biotin in the S4 and S5 binding sites, respectively. The arrangement of Phe166,

Table 2. Rates of Inhibition of *hum*PR3 by Peptide Phosphonates

$$E + I \underset{K_i}{\rightleftharpoons} EI \underset{k_{-2}}{\overset{k_2}{\rightleftharpoons}} E\text{-}I$$

Initial non-covalent complex   Final covalent complex

1	
Ac-**Pro**-Tyr-Asp-**Ala**P(O-C$_6$H$_4$-4-Cl)$_2$	
K_i (nM)	3600 ± 425
k_2 (min^{-1})	0.08 ± 0.01
2	
Bt-**Pro**-Tyr-Asp-**Ala**P(O-C$_6$H$_4$-4-Cl)$_2$	
K_i (nM)	21 ± 4.2
k_2 (min^{-1})	0.035 ± 0.01
11	
Bt-**Val**-Tyr-Asp-**nVal**P(O-C$_6$H$_4$-4-Cl)$_2$	
K_i (nM)	5.4 ± 0.14
k_2 (min^{-1})	0.15 ± 0.01

Table 3. Kinetics of Synthetic Substrate Cleavage by *hum*PR3 and *hum*NE

		proteases	
		k_{cat}/K_m $(M^{-1}\ s^{-1})^a$	
pNA substrates	[S] mM	*hum*PR3	*hum*NE
Ac-Pro-Tyr-Asp-Ala-pNA	1	4201 ± 29.7^b	nh
Bt-Pro-Tyr-Asp-Ala-pNA	1	25080 ± 141.4	nh
Bt-**Val**-Tyr-Asp-Ala-pNA	1	34965 ± 99	nh
Bt-**Val**-Tyr-Asp-**nVal**-pNA	1	80510 ± 2973	nh

^{a}Values are means $\pm$ SD of three experiments. ^{b}Value was taken from ref 18. Definition of abbreviation: nh, not hydrolyzed

Cys168, and Arg177 residues in the S5 subsite creates the cavity that accommodates the biotin heterocyclic rings (Figure 2B). The stabilizing role of biotin was confirmed by introducing a polyethylene glycol [PEG]$_2$ spacer between the P4 residue Pro and biotin (Bt-[**PEG**]$_2$-PYDA^P(O-C$_6$H$_4$-4-Cl)$_2$ (**3**), which resulted in a dramatic fall of the $k_{obs}/[I]$ (Table 1). The docking model shows that the length of the biotin moiety is optimal for the binding in the S5 pocket, and any spacer between the Pro4 and biotin would not improve the interaction. A biotin at P5

A
1
Ac-Pro-Tyr-Asp-Ala^P(O-C$_6$H$_4$-4-Cl)$_2$

*hum*PR3

B
2
Bt-Pro-Tyr-Asp-Ala^P(O-C$_6$H$_4$-4-Cl)$_2$

*hum*PR3

C
8
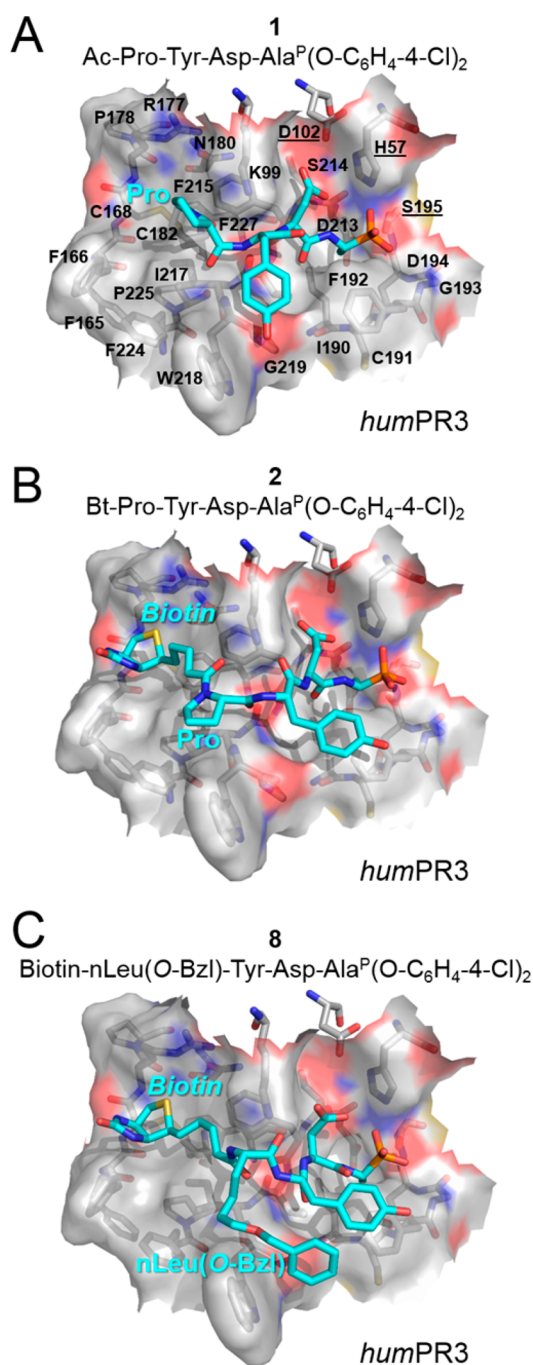Biotin-nLeu(*O*-Bzl)-Tyr-Asp-Ala^P(O-C$_6$H$_4$-4-Cl)$_2$

*hum*PR3

Figure 2. Proposed putative model of **1** (A), **2** (B), and **8** (C) binding to the active site of *hum*PR3. The solvent-accessible surface area of the active site in *hum*PR3 (PDB 1FUJ[12]) was made transparent to allow the visualization of the residues in stick representation. The single-letter code of residues in the vicinity of the active site is indicated in black. Residues are labeled following the numbering of chymotrypsin. The residues of the catalytic triad H57, D102, and S195 are underlined. The carbon atoms of PR3 and the compounds are shown in white and cyan, respectively. The oxygen, nitrogen, sulfur, and phosphorus atoms are colored in red, blue, yellow, and orange, respectively.

---

was thus retained for the construction of new inhibitors with a modified peptidyl sequence.

Influence of the P4 Residue on the Inhibitory Activity of Bt-Peptidyl^P(O-C$_6$H$_4$-4-Cl)$_2$ Phosphonate Inhibitors. The computational docking study showed that the P4 residue

Pro in **2** was close to solvent accessible hydrophobic Trp218 in PR3 (Figure 2B). We replaced the P4 Pro by Val (**4**), Leu (**5**), Ile (**6**), and norleucine (nLeu) (**7**) to tentatively optimize the interaction with the PR3 hydrophobic patch build by residues Phe166, Ile217, Phe224, and possibly with Trp218. While Leu or Ile at P4 position decreased the inhibitory activity toward PR3, the presence of nLeu or Val improved the inhibitory activity by ~2 and ~4 times, respectively (Table 1). Accordingly, the specificity constant k_{cat}/K_m of the pNA substrate Bt-VYDA-pNA was also improved (Table 3). Whatever the substitution at P4 in phosphonate inhibitors was, the resulting compound retained no significant inhibitory activity toward *hum*NE although this protease also prefers a hydrophobic residue at this position. Because the S4 subsite is composed mainly by side chains of Trp218 and Ile217 and the distinctly hydrophobic area (Phe166, Phe224) span beyond this position, we decided to probe the existence of interactions by substitution nLeu by nLeu(*O*-Bzl) at P4 in **7** (**8**). However, this resulted in more than 10 times lower $k_{obs}/[I]$ value (Table 1). Moreover, the molecular docking model did not confirm the interaction between nLeu(*O*-Bzl) and, as mentioned above, a distant hydrophobic area. In fact, the P4 side chain of **8** makes contact mainly with Trp218 (Figure 2C). The comparison with the **2** model (Figure 2B) indicates that the introduction of more sizable nLeu(*O*-Bzl) group at P4 does not alter the overall mode of binding but affects the placement of inhibitor backbone at the S4 subsite, thus preventing hydrogen bond formation between Lys99 and the carbonyl oxygen of the Bt-nLeu(*O*-Bzl) amide (Figure 1C).

Influence of the P1 and P4 Residues on the Efficacy of Bt-Peptidyl^P(O-C$_6$H$_4$-4-Cl)$_2$ Phosphonate Inhibitors. Unlike the S2 subsite of PR3 that preferentially accommodates negatively charged P2 residues and is thus essential to confer PR3 selectivity,[15] the S1 subsite in PR3 may accommodate a variety of residues including norvaline (nVal) and aminobutyric acid (Abu) among the favorites. We substituted the P1 alanyl residue in the parent inhibitor (**2**) by Abu and nVal. Bt-PYDA^P(O-C$_6$H$_4$-4-Cl)$_2$ (**2**) and Bt-PYD**Abu**^{P}(O-C$_6$H$_4$-4-Cl)$_2$ (**9**) showed similar efficacy toward PR3 (Table 1). However, Bt-PYD**nV**^{P}(O-C$_6$H$_4$-4-Cl)$_2$ (**10**) was ~4.5 times more potent than **2**.

As expected, the substitution of Pro by Val at P4 in **10** (**11**) significantly improved the $k_{obs}/[I]$ value, providing the best inhibitor of the series with a $k_{obs}/[I] = 73000 \pm 5000$ M^{-1} s^{-1}. This 20-fold increase as compared to **1** resulted from a decrease in the K_i value of the initial equilibrium between PR3 and Bt-**VYDnV**^{P}(O-C$_6$H$_4$-4-Cl)$_2$ (**11**) and an increase of the first-order rate constant k_2 producing the final covalent complex (Table 2). Combining Val at P4 and nVal at P1 in the pNA substrate Bt-VYDnV-pNA also significantly increased the specificity constant toward PR3 (Table 3).

The computational docking approach employed to examine the interaction between Bt-**VYDnV**^{P}(O-C$_6$H$_4$-4-Cl)$_2$ and *hum*PR3 (Figure 3A) revealed that for the lowest energy pose the overall mode of enzyme–inhibitor binding resembles the one obtained for Bt-**PYDA**^{P}(O-C$_6$H$_4$-4-Cl)$_2$ (**2**). The biotin aliphatic chain interacts with the hydrophobic surface of S5 subsite, while the biotin rings extend into the terminal cavity of this subsite in the manner observed with Bt-**PYDA**^{P}(O-C$_6$H$_4$-4-Cl)$_2$. For both models, the P4 residue of inhibitor is located at the narrow subsite with the Trp218 on one side and the Lys99 on the other. Therefore, increased inhibitory potency observed for derivatives with Val instead of Pro at P4 may be due to an
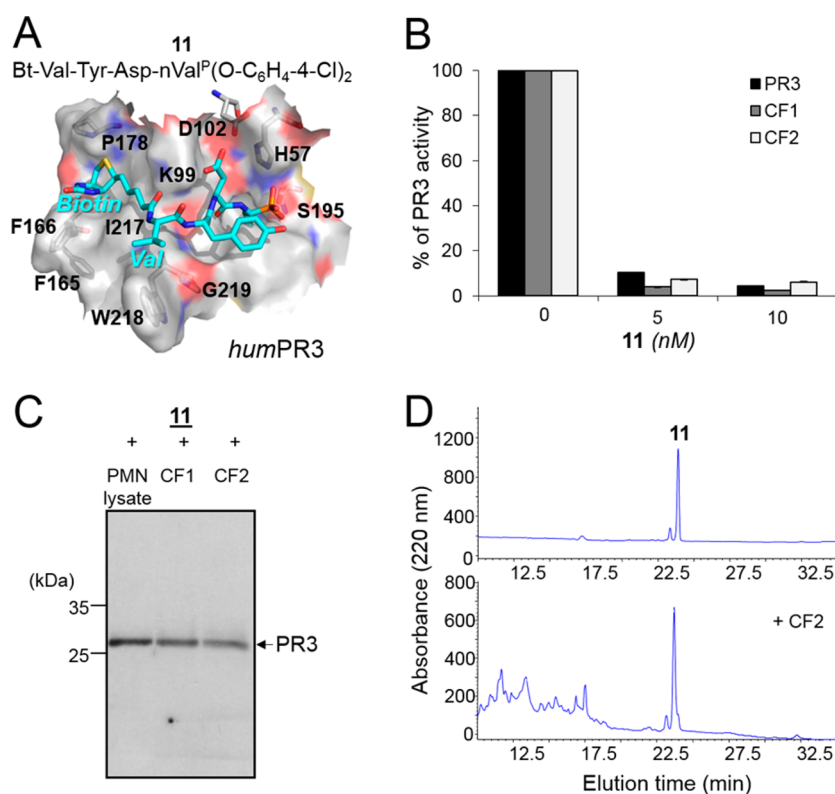
Figure 3. Inhibition of *hum*PR3 and stability of **11** in the cell free supernatants of sputa from CF patients. (A) Proposed putative model of **11** in *hum*PR3 active center. (B) Inhibition of PR3 in a representative CF sputum supernatants. The volume of CF sputum was adjusted to give final concentrations of PR3, 1 nM. Diluted samples were incubated with **11** (5 and 10 nM final) for 20 min at 37 °C. Inhibition was monitored by measuring the residual activity of PR3 on ABZ-VADnVADYQ-EDDnp (20 μM). Purified PR3 (1 nM) was used as control. (C) Selective labeling of PR3 activity in CF sputum and neutrophil lysate. Samples (10 μg of total protein) were incubated for 20 min at 37 °C with **11** (50 nM), and the mixtures were analyzed by WB using extravidin-peroxidase. (D) HPLC profile of the **11** after a 120 min incubation time with samples showing the stability of the inhibitor in sputa from cystic fibrosis patients. Similar results were found in three independent experiments.

234 improved flexibility of this region upon enzyme–inhibitor
235 binding. The ε-amino group of Lys99 forms hydrogen bonds
236 with Bt-Val4 amide carbonyl oxygen as well as Asp2 carboxyl
237 group. Additionally, quantum chemical calculations of inter-
238 action energy revealed that Lys99 residue contributes the most
239 to binding of Bt-Val4 portion of the inhibitor, as the value of
240 the interaction energy due to the presence of this particular
241 residue amounts to −16.6 kcal/mol (Table 4). Attracting
242 interactions between Bt-Val4 tail of **11** and PR3 residues were
243 also found for Phe166 and Val216 (−3.8 and −1.6 kcal/mol,
244 respectively). Except for Ile217, Trp218, and Phe215 residues
245 that appear to exert unfavorable influence in terms of Bt-Val4
246 binding, the remaining PR3 residues promote Bt-Val4 binding
247 with the interaction energy not exceeding −1 kcal/mol. It
248 should be pointed out that excessively repulsive interactions
249 associated with some residues probably arise from the lack of
250 quantum chemical refinement of the binding poses obtained
251 from docking simulations, as empirical force field based
252 methods often employed throughout the docking procedures
253 tend to introduce shortened intermolecular contacts.[28] The
254 location of the biotin rings into the S5 binding site prevents
255 recognition of all these compounds by extravidin by Western
256 blotting (WB) under nondenaturing/reducing conditions
257 (not shown).

258 **Stability of Bt-VYDnV^P(O-C$_6$H$_4$-4-Cl)$_2$ (11) in a Bio-**
259 **logical Environment.** We then tested the properties of **11** in
260 sputa from patients with cystic fibrosis (CF) and measured
261 *hum*PR3 activities of sputum samples before and after

Table 4. MP2/6-31+G(d) Interaction Energy[a] between Amino Acid Residues Representing *hum*PR3 or *mac*PR3 Binding Site and Bt-Val4 Fragment of 11

		binding energy	
*hum*PR3 residues	substituted *mac*PR3 residues	*hum*PR3	*mac*PR3
Lys99		−16.6	−10.0
Phe165	Leu	−0.3	−0.4
Phe166	Leu	−3.8	−0.8
Cys168-Cys182		−0.8	−1.2
Asn98-Arg177-Asn180		−0.8	0.3
Pro178	Thr	0.1	0.2
Phe192		−0.1	0.0
Phe215		5.5	24.2
Val216		−1.6	−2.6
Ile217		12.3	15.4
Trp218	Arg	7.6	6.4
Gly219	Glu	−0.3	−3.3
Phe224		−0.6	−0.9
Pro225		−0.6	−0.7
Phe227		−0.8	−1.6

[a] In units of kcal/mol.

incubation with **11** (5−10 nM final). A 1 nM *hum*PR3 262
concentration was estimated in these samples by comparison 263
with the rate of hydrolysis of the ABZ-VADnVADYQ-EDDnp 264
substrate. Cleavage of the *hum*PR3 substrate was totally 265
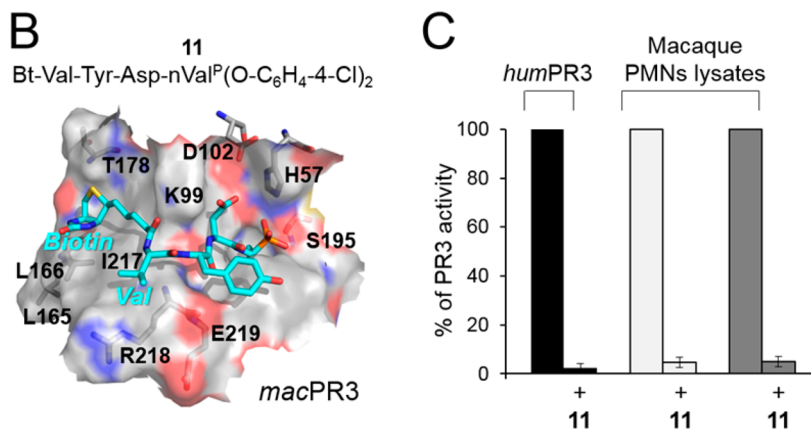inhibited after incubation for 20 min at 37 °C with **11** (Figure 266

Figure 4. Inhibition of *mac*PR3 by inhibitor **11**. (A) Human and macaque sequence alignment. The sequences of *hum*PR3 (1FUJ.pdb)[12] and *mac*PR3 (*Macaca fascicularis*, GenPept: XP_005587394.1) were aligned using Protein BLAST with default parameters. Similar amino acid residues are indicated in blue and remaining substitutions are in red. Active center residues are indicated by asterisk. The residues included in quantum chemical calculations are indicated in bold. The sequence numbering according 1FUJ.pdb file. Sequence alignment of *hum*PR3 and *mac*PR3 show 190/221 (86%) identical positions, 200/221 (90%) positives, and no gaps. (B) Proposed putative model of **11** in *mac*PR3 active center. (C) Inhibition of PR3 by **11** in macaque neutrophil lysates. The volume of lysates was adjusted to give final concentrations of PR3, 1 nM. Diluted samples were incubated with **11** (10 nM final) for 20 min at 37 °C. Inhibition was monitored by measuring the residual activity of PR3 on ABZ-VADnVADYQ-EDDnp (20 μM) as in Korkmaz et al.[52] Purified *hum*PR3 (1 nM) was used as control. Similar results were found in three independent experiments.

3B), while *hum*NE activity remained unchanged (not shown). Inhibitor **11** was also successfully used to selectively label proteolytically active *hum*PR3 in CF sputum and in a lysate of purified human blood neutrophils (Figure 3C). Additionally, we showed that inhibitor **11** preserved full inhibitory activity and resisted degradation when it was mixed with CF sputum for 2 h at 37 °C as shown by high performance liquid chromatography (HPLC) (Figure 3D).

Characterization and Inhibition of Macaque PR3 (*mac*PR3) by Phosphonate Inhibitors in Purified Neutrophil Lysates. Protein sequences alignment of *hum*PR3 and macaque PR3 (*Macaca fascicularis*) shows that they are 86% identical, and they differ by only 28 residues. Their substrate binding site is very similar and critical residues Lys99, Arg143, and Ile217 that confer high selectivity to *hum*PR3 are conserved in *mac*PR3 (Figure 4A,B). We thus hypothesized that, unlike PR3 homologues in rodents, *mac*PR3 will be efficiently inhibited by peptide-based phosphonate inhibitors designed for *hum*PR3. All phosphonate inhibitors of *hum*PR3 reported above were able to inhibit *mac*PR3. As observed for *hum*PR3, biotinylated inhibitors were more efficient than acylated inhibitors at inhibiting *mac*PR3 (**1**, Ac-PYDA^P(O-C$_6$H$_4$-4-Cl)$_2$, k_{obs}/I = 55 ± 4 M^{-1} s^{-1}; **2**, Bt-PYDA^P(O-C$_6$H$_4$-4-Cl)$_2$, k_{obs}/I = 1985 ± 215 M^{-1} s^{-1}; **11**, Bt-VYDA^P(O-C$_6$H$_4$-4-Cl)$_2$, k_{obs}/I = 36480 ± 3350 M^{-1} s^{-1}), but their overall potency was somewhat lesser than that recorded for *hum*PR3 (Table 1). The inhibition of *mac*PR3 with **11** is shown in Figure 3C.
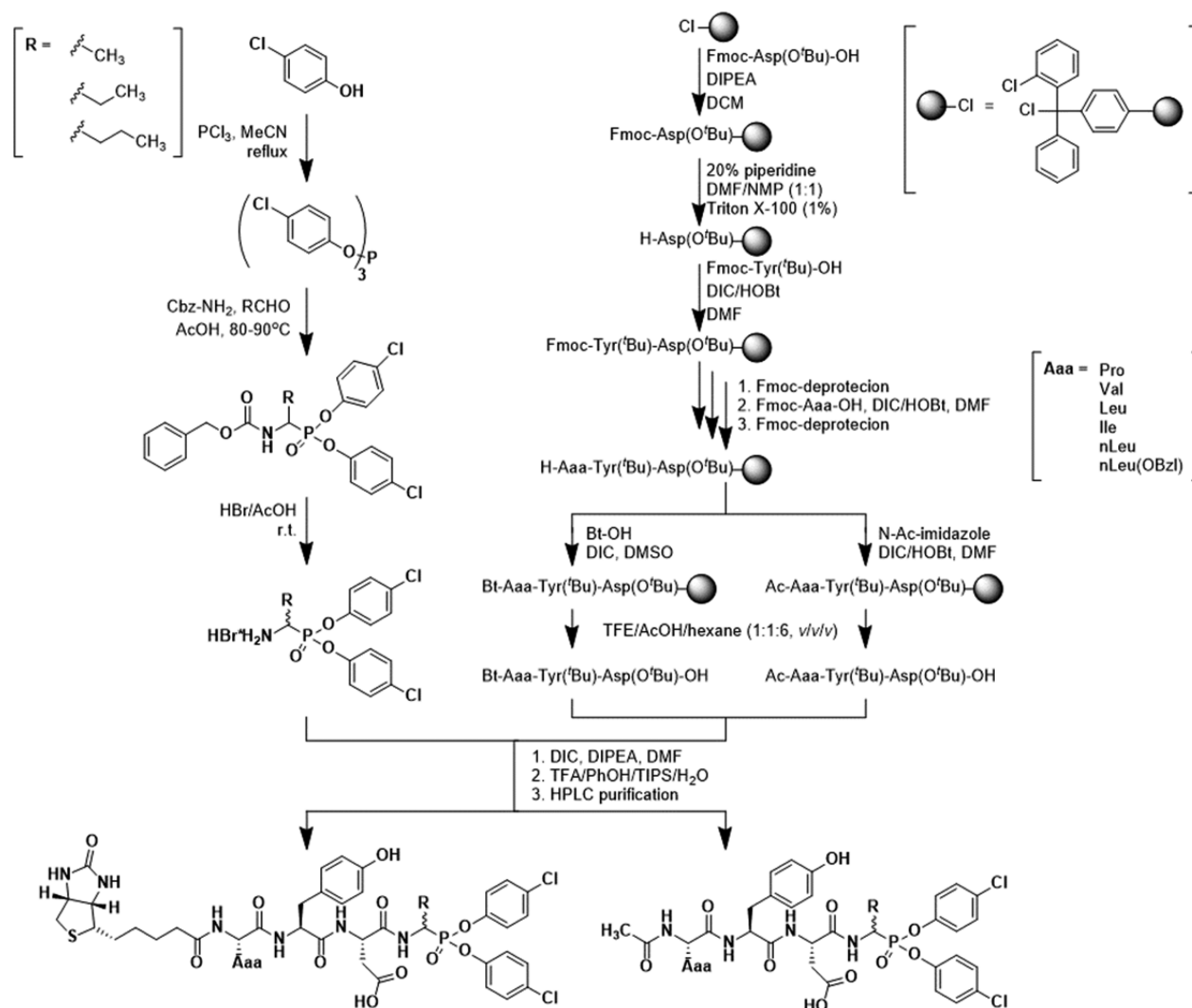
Figure 5. Scheme showing the synthesis of peptidyl di(chlorophenyl)-phosphonate ester inhibitors.

To further examine binding preferences of **11** against human and *mac*PR3 proteases and interaction energy values between Bt-Val4 fragment of the inhibitor and PR3, binding sites were compared for particular residues representing S5 binding pocket (Table 4). Lys99, the most important residue promoting inhibitor binding of *hum*PR3, seems to exert also the largest influence in terms of the analogous interaction with *mac*PR3. However, the corresponding binding energy value is less significant in the case of *mac*PR3–inhibitor complex compared to interaction with *hum*PR3 (−10.0 versus −16.6 kcal/mol; Table 4). Another substantial difference in binding energy values concerns repulsive interaction due to the presence of Phe215 residue. Unfavorable interaction characterizing *hum*PR3–inhibitor complex (5.5 kcal/mol) amounts to 24.2 kcal/mol in the corresponding *mac*PR3 Phe215–inhibitor complex (Table 4). The remaining repulsive interactions associated with Ile217 and Trp218 are retained in the case of *mac*PR3 inhibition despite the substitution of Trp218 by an arginine residue. Interestingly, three out of five substitutions that involve PR3 residues in the vicinity of the Bt-Val4 inhibitor fragment do not seem to modulate binding potency of **11** against human and *mac*PR3 homologues. The more substantial changes related to residue substitution accompany the change of Phe166 to leucine and Gly219 to glutamate. However, these substitution-induced changes in binding energy cancel each other out, as the interaction energy value increased by 3 kcal/mol as a result of the Phe166Leu substitution is decreased by the same extent upon the Gly219Glu substitution. Overall, the differences in inhibitor binding by human and *mac*PR3 appear to arise from decreased attractive interaction with Lys99 and increased repulsion with Phe215 residues. Because conformation and spatial placement of these two residues is essentially identical in both complexes, the observed changes in binding energy appear to arise from slightly different positioning of the Bt-Val4 portion of the inhibitor molecule due to substitutions present in the *mac*PR3 S4 and S5 subsites.

■ DISCUSSION

Evidence has now accumulated that the neutrophilic serine protease *hum*PR3 acquired specific pathophysiological properties and nonredundant functions in spite of its close resemblance to *hum*NE.[5,29] Indeed, it slightly differs from the latter by its spatiotemporal localization,[30] its substrate specificity, and its sensitivity to natural inhibitors, all factors that taken together explain its specific function as an autoantigen in granulomatosis with polyangiitis and its probable involvement in cell apoptosis.[6,11] Controlling the proteolytic activity of this protease specifically, e.g., by protease inhibitors,

is a means to better understand its biological function, but all physiological inhibitors of *hum*PR3 preferentially target *hum*NE. It is only recently that we and others began to synthesize chemical inhibitors that selectively target the *hum*PR3 active site.[7] The specificity of serine proteases is determined by their substrate binding sites that are located on both sides of the cleaved peptide bond. We used a substrate-based approach to develop serpin-like irreversible inhibitor (SerpinB1(STDA/R)) and azapeptide (azapro-3), a reversible inhibitor that selectively inhibits PR3.[31] Such inhibitors, however, cannot be used as ABP to visualize active *hum*PR3 in biological fluids or in cells and tissues. We recently developed a series of N-terminally biotinylated peptidyl-diphenyl phosphonate inhibitors that allow the detection of *hum*PR3 at the cell surface and inside cells.[18] These are transition state analogues, irreversible inhibitors that interact with nonprime subsites of the target serine protease to form "phosphonylated" enzymes. Protease−inhibitor complexes show a remarkable stability due to the similarity of the phosphorus atom with the tetrahedral intermediate formed during peptide bond hydrolysis. Although chemically stable in blood samples, their pharmacological use requires that they interact rapidly with their target protease to be effective at low concentrations. We have further investigated the nonprime specificity of *hum*PR3 to develop more potent di-(chlorophenyl)-phosphonate ester inhibitors that could be used as molecular probes to control *hum*PR3 activity (Figure 5).

We previously showed that the S2/P2 specificity was essential to discriminate between *hum*PR3 and its close homologue *hum*NE.[15] Lys99 in *hum*PR3 is a key residue to explain the preferential accommodation of negatively charged or polar residues at P2.[5,7] Thus, selective *hum*PR3 substrates or peptide sequences selectively cleaved by *hum*PR3 all contain a negatively charged or a polar residue at position P2.[6] SerpinB1(STDA/R) and azapro-3 that selectively inhibit *hum*PR3 contain a negatively charged residue (Asp) at P2 position. However, *hum*PR3 may accommodate different residues at P1 and P4 as confirmed by molecular modeling studies. The S1 binding pocket of *hum*PR3 is more accessible and spacey than that of *hum*NE and can accommodate not only the Ala or Abu side chain but also methionine, valine, and nVal, which was shown experimentally and by computational docking. In a recent study using single-residue mutant of *hum*PR3 with Arg at position 217 (PR3I217R), we showed that Ile217 located in the neighborhood of the S4 subsite pocket significantly affects the substrate specificity of *hum*PR3.[18] The docking models performed in this study using phosphonate inhibitors indicate also that the solvent accessible surface of the S4 subsite is limited by Trp218 and Ile217 on one side. The latter two residues are most likely responsible for the binding preference toward aliphatic side chains at P4 and Lys99, which is located on the opposite side of the S4 subsite, determines cooperation between S2 and S4 via hydrogen bonding. Introduction of a Val and a nVal at P4 and P1 positions, respectively, in the biotinylated *hum*PR3 inhibitor previously reported, Bt-PYDA^P(O-C$_6$H$_4$-4-Cl)$_2$ (**2**), enhanced the $k_{obs}/[I]$ value toward *hum*PR3 by ∼20-fold. This was probably because the substitution of Pro4 by Val4 improved the flexibility of the inhibitor, favoring the formation of hydrogen bonds between the ε-amino group of Lys99 and Bt-Val4 amide carbonyl oxygen as well as Asp2 carboxyl group. These hydrogen bond interactions are in agreement with previously described cooperation observed between S2 and S4 subsites.[18]

Biotin at the N-terminal of P4 residue in phosphonate inhibitors and peptidyl-pNA substrates displays stabilizing properties. General orientation, size, and hydrophobic character of *hum*PR3 S5 pocket that accommodates N-terminal biotin is similar to that of *hum*NE crystallized in complex with a phosphonate inhibitor bearing a nLeu(*O*-Bzl) moiety at P4 and called an "exopocket", an extension of the S4 subsite.[32] The docking models from this study show that the terminal cavity of the *hum*PR3 S5 pocket formed by Phe166, Cys168, and Arg177 accommodates the biotin heterocyclic rings, while the hydrophobic surface of Ile217 interacts with the biotin aliphatic chain. The location of the biotin rings into the S5 binding site prevents recognition of the biotinylated inhibitors by extravidin by WB under nondenaturating conditions (not shown). Only the five-carbon aliphatic chain of biotin participates in the stabilization of the inhibitor within the *hum*PR3 active site as deduced from the observation that a phosphonate inhibitors with a same peptide sequence but bearing only a N-terminal five-carbon aliphatic chain enhanced the inhibition rate as well as whole biotin.[18] Analysis of the docking models suggests that the substantial impact of N-terminal biotin binding with S5 subsite on the overall inhibitory potency might be connected with the limited size of S4 binding site. The main contribution to the binding energy at this position is provided by Lys99, forming the hydrogen bond with the backbone of the inhibitor and stabilizing the biotin moiety in proper orientation. Because of the narrow character of S4 subsite and the presence of Trp218 and Ile217 on the opposite site of Lys99, there is a strong preference for small, hydrophobic residues at P4 position. Therefore, the introduction of more sizable side chain such as nLeu(*O*-Bzl) may influence proper stabilization of the compound at P4 subsite, resulting in decreased inhibitory potency.

One of the challenges when designing preclinical studies for PR3 is to select a relevant animal model. We previously showed that PR3 from rodents differs from *hum*PR3 both in terms of substrate specificity, which preclude the use of substrate-derived phosphonate inhibitors and of subcellular distribution because there is no constitutive expression of PR3 at the neutrophil surface of rodent neutrophils.[27,33] We therefore used a nonhuman primate model to investigate the substrate specificity of neutrophilic PR3 and its sensitivity to phosphonate inhibitors developed against *hum*PR3. In view of the highly conserved primary amino acid sequence of *mac*PR3 implying a very similar specificity as with *hum*PR3, *mac*PR3 cleaved the *hum*PR3 substrate at the same site[34] and this activity was inhibited by all phosphonate inhibitors of *hum*PR3 used in this study. WB analysis of the macaque neutrophil lysate using an anti-*hum*PR3 antibody revealed the presence of a single band of 26 kDa in the neutrophil lysate with no glycosylated forms.[34] A single band of 75 kDa was revealed after the lysate was incubated with human α1PI, indicating that *mac*PR3 had formed an irreversible complex with the serpin. In keeping with this observation, the proteolytic activity toward the *hum*PR3 substrate in the lysate was inhibited by α1PI and by the PR3-specific serpinB1(STDA/R) inhibitor[35] (not shown). The identification of proteolytically active *mac*PR3 in the neutrophil lysate was further confirmed by electrophoresis under nondenaturing/nonreducing conditions using the ABP Bt-[PEG]66-PYDAP(O-C$_6$H$_6$-4-Cl)$_2$ and streptavidin-peroxidase staining.[34] We found similar level of active PR3 in lysates

of purified human and macaque neutrophils by kinetics and immunoblotting assays. The macaque model thus appears as relevant animal model for in vivo studies.

■ CONCLUSION

Targeting the *hum*PR3 active site by specific inhibitors has become evidence as soon as it has been established that it was not a redundant protease mimicking *hum*NE and that its proteolytic activity was poorly controlled by physiological inhibitors. We have optimized here the structure of peptidyl phosphonate inhibitors by coupling molecular modeling studies with kinetic analyses, and we obtained molecular probes to follow the fate and further investigate the function of PR3 both in vitro and in vivo. The potency and selectivity of the inhibitors developed here let us suppose that they are suitable therapeutic tools for fighting inflammatory and/or infectious diseases where the role of *hum*PR3 has been clearly identified or even only suspected.

■ EXPERIMENTAL SECTION

Materials. *hum*NE (EC 3.4.21.37) was obtained from Athens Research and Technology (USA). The fluorescence resonance energy transfer (FRET) substrates ABZ-VADnVADYQ-EDDnp/ABZ-APEEIMRRQ-EDDnp and chromogenic *para*-nitroanilide substrates synthesized by Genecust (Dudelange Luxembourg). IGEPAL CA-630 (NP40) was purchased from Sigma-Aldrich (St. Louis, MO, USA).

Synthesis of Peptidyl-phosphonate Inhibitors. All reagents and solvents were obtained from commercial sources and were used without purification.

All final compounds were purified to >95% purity HPLC system (Jasco LC System, Jasco, Japan) equipped with Supelco Wide Pore C8 column (8 mm × 250 mm) and ultraviolet−visible (UV−vis, 226 nm) and fluorescent detectors (excitation 320 nm, emission 450 nm). A linear gradient from 10 to 90% of B within 40 min was applied (A, 0.1% TFA in water; B, 80% acetonitrile in A).

The nuclear magnetic resonance spectra (^{1}H, ^{31}P and ^{13}C) were recorded on either a Bruker Avance DRX-300 (300.13 MHz for ^{1}H NMR, 121.50 MHz for ^{31}P NMR), a Bruker Avance 600 MHz (600.58 MHz for ^{1}H NMR, 243.10 MHz for ^{31}P NMR, and 101.12 MHz for ^{13}C NMR) or Bruker AVANCE III 700 MHz (700.67 MHz for ^{1}H NMR) spectrometer. Chemical shifts are reported in parts per million (ppm) relative to a tetramethylsilane internal standard. Mass spectra were recorded using a Biflex III MALDI TOF mass spectrometer (Bruker, Germany). The cyano-4-hydroxycinnamic acid (CCA) was used as a matrix. High resolution mass spectra (HRMS) were acquired either on a Waters Acquity Ultra Performance LC, LCT Premier XE, or Bruker micrOTOF-Q II mass spectrometer.

Cbz-Protected 1-Aminoalkylphosphonate Diaryl Esters (General Procedure). The first step in the synthesis of the phosphonic analogues of Ala, nVal, and Abu was the preparation of tri(4-chlorophenyl)phosphite from 4-chlorophenol and phosphorus trichloride.[36] Briefly, phosphorus trichloride (10 mmol) was added to 4-chlorophenol (30 mmol) dissolved in acetonitrile (50 mL) and the mixture refluxed for 6 h. The volatile elements were removed in a vacuum, and the resulting crude phosphite, a yellow oil, was used directly in an amidoalkylation reaction. It was mixed with benzyl carbamate (12 mmol) and an appropriate aldehyde: acetaldehyde, butyraldehyde, or propionaldehyde (12 mmol) and refluxed in acetic acid for 3 h (Oleksyszyn's method[37]).

Deprotection of Cbz Group (General Procedure). The Cbz protecting group was removed by incubation with 33% hydrobromic acid in acetic acid (2 h). The volatile components were removed under reduced pressure, and the products were crystallized from methanol/diethyl ether to give target compounds as hydrobromide salts.

Benzyl (1-(Bis(4-chlorophenoxy)phosphoryl)ethyl)carbamate (12, Cbz-Ala^P(O-C$_6$H$_4$-4-Cl)$_2$). **12** was prepared using the general method described above and crystallized from methanol to yield a white solid (56%). ^{1}H NMR (300.13 MHz, CDCl$_3$-d_1, ppm): δ 7.43−6.97 (m, 14H), 5.22−5.08 (m, 2H), 4.74−4.37 (m, 1H), 1.56 (dd, *J* = 18.2, 7.4 Hz, 3H). ^{31}P NMR (121.50 MHz, CDCl$_3$-d_1, ppm): δ 19.56 (s). ^{13}C NMR (101.12 MHz, DMSO-d_6, ppm): δ 156.16, 156.11, 151.14, 151.05, 150.84, 150.74, 137.20, 134.14, 131.91, 131.88, 128.87, 128.46, 128.34, 126.15, 126.03, 121.13, 121.09, 120.99, 119.99, 119.73, 66.48, 45.30, 43.73, 15.52. HRMS: calcd for (C$_{22}$H$_{20}$Cl$_2$NO$_5$P)H$^+$ 480.0534, found 480.0533.

Benzyl (1-(Bis(4-chlorophenoxy)phosphoryl)propyl)carbamate (13, Cbz-Abu^P(O-C$_6$H$_4$-4-Cl)$_2$). **13** was prepared using the general method described above and crystallized from methanol to yield a white solid (19%). ^{1}H NMR (300.13 MHz, CDCl$_3$-d_1, ppm): δ 7.45−6.99 (m, 13H), 5.14 (d, *J* = 10.7 Hz, 1H), 5.24−5.06 (m, 2H), 4.50−4.33 (m, 1H), 2.20−2.03 (m, 1H), 1.87−1.64 (m, 1H), 1.11 (t, *J* = 7.3 Hz, 3H). ^{31}P NMR (121.50 MHz, CDCl$_3$-d_1, ppm): δ 18.31 (s). ^{13}C NMR (101.12 MHz, DMSO-d_6, ppm): δ 156.85, 156.81, 149.45, 149.35, 149.12, 149.03, 137.34, 130.35, 130.28, 130.03, 129.86, 129.65, 128.88, 128.44, 128.32, 128.01, 122.94, 122.90, 122.67, 122.63, 117.44, 66.43, 51.27, 49.72, 22.46, 22.42, 11.16, 11.01. HRMS: calcd for (C$_{23}$H$_{22}$Cl$_2$NO$_5$P)H$^+$ 494.0691, found 494.0699.

Benzyl (1-(Bis(4-chlorophenoxy)phosphoryl)butyl)carbamate (14, Cbz-nVal^P(O-C$_6$H$_4$-4-Cl)$_2$). **14** was prepared using the general method described above and crystallized from methanol to yield a white solid (20%). ^{1}H NMR (600.58 MHz, CDCl$_3$-d_1, ppm): δ 7.42−6.68 (m, 13H), 5.24−5.15 (m, 2H), 5.11 (d, *J* = 12.2 Hz, 1H), 4.57−4.44 (m, 1H), 2.07−1.95 (m, 2H), 1.67−1.39 (m, 2H), 1.02−0.93 (m, 3H). ^{31}P NMR (243 MHz, CDCl3, ppm): δ 18.47 (s). ^{13}C NMR (101.12 MHz, DMSO-d_6, ppm): δ 156.85, 156.76, 156.71, 149.45, 149.35, 149.11, 149.02, 137.32, 130.36, 130.29, 130.05, 129.87, 129.65, 128.88, 128.45, 128.34, 122.95, 122.91, 122.67, 122.63, 117.44, 66.44, 49.23, 47.66, 30.63, 19.10, 18.95, 13.68. HRMS: calcd for (C$_{24}$H$_{24}$Cl$_2$NO$_5$P)Na$^+$ 530.0667, found 530.0670.

Bis(4-chlorophenyl) (1-Aminoethyl)phosphonate Hydrobromide (15, HBr×H$_2$N-Ala^P(O-C$_6$H$_4$-4-Cl)$_2$). **15** was prepared using the general method described above and crystallized from diethyl ether to yield a white solid (97%). ^{1}H NMR (300.13 MHz, DMSO-d_6, ppm): δ 8.85 (s, 3H), 7.57−7.44 (m, 4H), 7.36−7.16 (m, 4H), 4.45−4.24 (m, 1H), 1.55 (dd, *J* = 18.3, 7.2 Hz, 3H). ^{31}P NMR (121.50 MHz, DMSO-d_6, ppm): δ 16.49 (s). ^{13}C NMR (101.12 MHz, DMSO-d_6, ppm): δ 148.63, 148.61, 148.53, 148.52, 130.57, 130.54, 130.53, 129.62, 123.02, 122.98, 122.94, 117.45, 43.50, 41.93, 13.96, 13.93. HRMS: calcd for (C$_{14}$H$_{14}$Cl$_2$NO$_3$P)H$^+$ 346.0167, found 346.0172.

Bis(4-chlorophenyl) (1-Aminopropyl)phosphonate Hydrobromide (16, HBr×H$_2$N-Abu^P(O-C$_6$H$_4$-4-Cl)$_2$). **16** was prepared using the general method described above and crystallized form diethyl ether to yield a white solid (83%). ^{1}H NMR (300.13 MHz, DMSO-d_6, ppm): δ 8.87 (s, 2H), 7.67−7.13 (m, 8H), 4.21 (dt, *J* = 13.6, 6.8 Hz, 1H), 2.24−1.74 (m, 2H), 1.11 (t, *J* = 7.4 Hz, 3H). ^{31}P NMR (121.50 MHz, DMSO-d_6, ppm): δ 16.50 (s). ^{13}C NMR (101.12 MHz, DMSO-d_6, ppm): δ 148.56, 148.47, 130.58, 130.54, 123.05, 123.01, 122.97, 122.93, 48.80, 47.26, 22.01, 21.99, 10.81, 10.72. HRMS: calcd for (C$_{15}$H$_{16}$Cl$_2$NO$_3$P)H$^+$ 360.0313, found 361.1123.

Bis(4-chlorophenyl) (1-Aminobutyl)phosphonate hydrobromide (17, HBr×H$_2$N-nVal^P(O-C$_6$H$_4$-4-Cl)$_2$). **17** was prepared using the general method described above and crystallized from diethyl ether to yield a white solid (89%). ^{1}H NMR (300.13 MHz, DMSO-d_6, ppm): δ 8.88 (s, 2H), 7.49−7.27 (m, 8H), 4.25 (dt, *J* = 13.9, 7.0 Hz, 1H), 2.06−1.78 (m, 2H), 1.71−1.46 (m, 2H), 0.90 (t, *J* = 7.3 Hz, 3H). ^{31}P NMR (121.50 MHz, DMSO-d_6, ppm): δ 16.55 (s). ^{13}C NMR (101.12 MHz, DMSO-d_6, ppm): δ 148.59, 148.58, 148.49, 148.48, 130.58, 130.53, 123.06, 123.02, 122.96, 122.92, 47.40, 45.85, 30.39, 30.36, 19.02, 18.92, 14.06. HRMS: calcd for (C$_{16}$H$_{18}$Cl$_2$NO$_3$P)H$^+$ 374.0474, found 375.1931.

The peptides were synthesized manually by the solid-phase method using Fmoc chemistry. The following amino acid derivatives were used: Fmoc-Pro, Fmoc-Val, Fmoc-Leu, Fmoc-Ile, Fmoc-nLeu, Fmoc-nLeu(O-Bzl), Fmoc-Tyr(tBu), and Fmoc-Asp(OtBu). The protected derivative of the C-terminal amino acid residue, Fmoc-Asp(OtBu), was attached to the 2-chlorotrityl resin (substitution of Cl 1.46 mequiv/g) (Calbiochem-Novabiochem AG, Switzerland) in the presence of an

equimolar amount of diisopropylethylamine (DIPEA) under anhydrous conditions in dichloromethane (DCM) solution. A peptide chain was elongated in consecutive cycles of deprotection (20% piperidine in dimethylformamide (DMF)/n-methylpyrrolidone (NMP) (1:1, v/v) with 1% Triton X-100) and coupling (DIC/HOBt chemistry; 3 equiv of protected amino acid derivatives were used). A 10-fold molar excess of N-acetylimidazole in DMF was used for acetylation of the N-terminus. Bt-[PEG]$_2$-Pro-Tyr-Asp-Ala^P(O-C$_6$H$_4$-4-Cl)$_2$ was synthesized via coupling of the Fmoc-PEG$_2$ to the amino group of terminal Pro residue. The N-terminal biotin group was conjugated using a 5-fold molar excess of biotin and 1,3-diisopropylcarbidiimide (DIC) as the coupling agent in anhydrous DMSO for 6 h at 30 °C. The synthesized peptides were cleaved from the resin with TFE/hexane/acetic acid (1:6:1, v/v/v).

Fully protected peptides were dissolved in DMF and their carboxyl groups were activated with DIC and coupled with HBr×H$_2$N-Ala^P(O-C$_6$H$_4$-4-Cl)$_2$, HBr×H$_2$N-Abu^P(O-C$_6$H$_4$-4-Cl)$_2$, or HBr×H$_2$N-nVal^P(O-C$_6$H$_4$-4-Cl)$_2$ in DMF in the presence of DIPEA. The mixture was stirred for 6 h, and the DMF was removed under reduced pressure. The resulting compounds were suspended in trifluoroacetic acid (TFA)/phenol/triisopropylsilane/H$_2$O (88:5:2:5, v/v/v/v) for 2 h to remove side chain protecting groups.

The crude peptides were purified by HPLC on a Beckman Gold System (Beckman, USA) with an RP Kromasil-100, C8, 5 μm column (8 mm × 250 mm) (Knauer, Germany). The solvent systems were 0.1% TFA (A) and 80% acetonitrile in A (B). Either isocratic conditions or a linear gradient were applied (flow rate 3.0 mL/min, monitored at 226 nm). The purity of the synthesized peptides was verified on RP Kromasil 100, C8, 5 μm column (4.6 mm × 250 mm) (Knauer, Germany). The peptides were eluted with a linear gradient of the above solvent system (10%−90% B) for 30 min, flow rate 1 mL/min, monitored at 226 nm. HPLC retention times and ^{1}H NMR spectra of final phosphonate peptide inhibitors are shown in Table 5

Table 5. Calculated and Observed Masses[a] and HPLC Retention Times of Synthesized Inhibitors 1−11

compd	calculated mass (Da)	found mass (Da)	retention time (min)
1	763.56	764.67	12.36
2	947.82	948.91	13.12
3	1266.18	1266.23	10.05
4	949.83	951.01	12.56
5	963.86	964.79	12.47
6	963.86	964.92	12.51
7	963.86	964.88	12.42
8	1055.95	1057.08	13.57
9	961.54	962.50	13.43
10	975.87	976.95	13.20
11	977.89	977.97	12.58

[a]The obtained molecular weights represent pseudomolecular ions (M + H)$^+$.

and Supporting Information, respectively. Mass spectrometric analysis of the inhibitors (Table 5) was done on a MALDI MS (a Biflex III MALDI-TOF spectrometer, Bruker Daltonics, Germany) using a CCA matrix.

Enzymatic Studies: Free humPR3 and humNE Were Titrated with α1PI.[38] k_{cat}/K_m determination: The specificity constants k_{cat}/K_m for peptidyl-pNA substrates were determined under first-order conditions.[38] The cleavage of the substrates (1 mM final) was monitored by measuring the absorbance of liberated pNA at 410 nm on the spectrophotometer (Versamax microplate reader, Molecular Devices, Sunnyvale, CA, USA). Measurements were carried out at 37 °C in buffer 50 mM HEPES, 0.75 M NaCl, 0.05% NP40, pH 7.4. Final protease concentrations were 0.01−1 μM.

$k_{obs}/[I]$ determination: The inactivation of proteases by phosphonate inhibitors (substrate analogue inhibitors) in the presence of the substrate by competition for the enzyme-binding site was measured by the method of Tian and Tsou.[39] Product formation in the presence of an irreversible inhibitor approaches an asymptote in this system, as described by $\log([P_\infty] - [P]) = \log[P_\infty] - 0.43A[Y]t$.

- where $[P_\infty]$ is the concentration of product formed at time approaching infinity, $[P]$ is the concentration of product at time t, $[Y]$ is the inhibitor concentration, and A is the apparent inhibition rate constant in the presence of the substrate. A is given by $A = k_{+o}/(1 + K^{-1}[S])$
- where k_{+o} is the rate constant for association of the inhibitor with the enzyme, K^{-1} is the inverted Michaelis constant, and $[S]$ the substrate concentration. The apparent inhibition rate constant A is the slope of a plot of $\log([P_\infty] - [P])$ against t, to give the second-order rate constant of inhibition k_{+o}.

The rates of inhibition of purified humPR3, macPR3 (in purified blood neutrophil lysates), and purified humNE were measured using FRET substrates (ABZ-VADnVADYQ-EDDnp (10 μM final) and ABZ-APEEIMRRQ-EDDnp (10 μM final) in 50 mM HEPES, 0.75 M NaCl, and 0.05% NP40, pH = 7.4; excitation wavelength, 320 nm; emission wavelength, 420 nm; Spectramax Gemini (Molecular Devices, Sunnyvale, CA, USA). Final protease concentrations were 1 nM.

K_i and k_2 determination: We monitored the extent of protease inhibition at several time points for a different inhibitor concentrations $[I]$. The observed rate constant for inhibition, k_{obs}, at each concentration was determined from the slope of a semilogarithmic plot of inhibition versus time. The k_{obs} values were replotted against inhibitor concentration and fitted to a hyperbolic equation, $k_{obs} = k_2[I]/(K_i + [I])$, to obtain values for K_i and k_2.[40]

Detection of PR3 in Biological Fluids. CF sputa (50 μg proteins) were incubated with 11 (50 nM final) for 20 min at 37 °C in PBS. The reaction was stopped by adding 1 volume of 2× SDS reducing buffer and heating at 90 °C for 5 min. The components of the mixture were separated by SDS-PAGE, 12% NaDodSO4-polyacrylamide gel electrophoresis under denaturing conditions. They were transferred to a nitrocellulose (Hybond)-ECL (Enhanced Chemiluminescence) membrane at 4 °C.

Extravidin Peroxidase Detection. Free sites on the membrane were blocked with 3% bovine serum albumin (BSA) in 0.1% Tween in PBS for 90 min at room temperature (RT). Membranes were then given two quick washes with PBS-Tween 0.1% and incubated for 2 h at RT with extravidin horseradish peroxidase (HRP) (Sigma-Aldrich) (diluted 1/4000 in 3% BSA in PBS-Tween 0.1%). The extravidin-HRP treated membrane was washed (3 × 10 min) with PBS-Tween 1% and then incubated with HRP substrate for 3 min. Reactive bands were identified by chemiluminescence (ECL Kit).

Immunodetection. Free sites on the membranes were blocked by incubation with 5% nonfat dried milk in PBS-0.1% Tween for 90 min at RT. They were washed twice with PBS-Tween 0.1% and incubated overnight with a rabbit primary anti-PR3 antibody (1:700, EPR6277 Abcam), followed by a goat antirabbit IgG secondary antibody (1:7000, A9169 Sigma). These membranes were then washed and processed as above.

Purification and Lysis of *M. fascicularis* Neutrophils. Female cynomolgus monkeys (*Macaca fascicularis*) (approximately 3 years old and weighing 4−5 kg) were obtained from a commercial supplier. All animal experiments and procedures were approved by the local animal experimentation ethics committee (Comité d'éthique Val de Loire (APAFIS no. 2982-20151105293399v6)). Five mL of peripheral blood samples were collected in lithium−heparin tubes from a femoral vein. Animals were kept under spontaneous ventilation during anesthesia with ketamine (10 mg/kg). The monitoring included pulse-oximetry and heart rate recording. Intravenous access was secured with a 22G canula on the legs. Anticoagulated whole blood was layered onto Ficoll density gradient and centrifuged. The purified neutrophils (>98%) in suspension was treated with H$_2$O for 30 s to lyse red blood cells. The neutrophils were then lysed in Hepes 50 mM, NaCl 0.15 M, NP40 0.5%, pH 7.4, and the supernatant was collected and stored at −80 °C.

Chromatographic Procedures and Peptide Analysis. Inhibitor 11 (75 μM final) was incubated with the cell free supernatants of sputa

from CF patients at 37 °C for 2 h in PBS. FRET substrate ABZ-VADnVADYQ-EDDnp[15] (20 μM final) was incubated with *hum*R3 and macaque neutrophil lysate supernatant (10−500 nM) at 37 °C in 50 mM HEPES, 0.75 M NaCl, and 0.05% NP40, pH = 7.4. The proteins were precipitated with absolute ethanol (4 volumes). The supernatant containing the peptides were dried under vacuum and dissolved in 200 μL of 0.01% trifluoroacetic acid (v/v), then fractionated by Agilent Technology 1200 series HPLC system (Agilent Technology, CA, USA) on a C18 column (2.1 mm × 30 mm, Merck Millipore) at a flow rate of 0.3 mL/min with a linear gradient (0−90%, v/v) of acetonitrile in 0.01% trifluoroacetic acid over 40 min. Eluted peaks were monitored at 220 nm.

Molecular Modeling. Molecular docking was performed in order to explain interactions of Ac-PYDA^P(O-C$_6$H$_4$-4-Cl)$_2$ (**1**), Bt-PYDA^P(O-C$_6$H$_4$-4-Cl)$_2$ (**2**), Bt-nLeu(*O*-Bzl)YDA^P(O-C$_6$H$_4$-4-Cl)$_2$ (**8**), and Bt-VYDnV^P(O-C$_6$H$_4$-4-Cl)$_2$ (**11**) with *hum*PR3 and *mac*PR3. As a receptor, the crystal structure of *hum*PR3 (1FUJ.pdb)[12] was selected. The same structure was used as a template for *mac*PR3 3D model obtained by means of automated homology modeling server, SWISS-MODEL.[41] For the docking studies, inhibitor molecules were used as a peptidyl phosphonic acids [Ac-PYDA^P(OH)$_2$, Bt-PYDA^P(OH)$_2$, Bt-VYDnV^P(OH)$_2$, and Bt-nLeu(*O*-Bzl)YDA^P(OH)$_2$] instead of di(chlorophenyl)-phosphonate esters, as this is the form present in the "aged" protein−inhibitor complex. The ligand models were optimized using the MM2 force field (as implemented in ChemBio3D 12.0),[42] while the atom types and protonation of all structures were set using SPORES.[43] The docking was carried out using the Protein−Ligand ANT System (PLANTS v. 1.2) with PLANTS$_{CHEMPLP}$ scoring function.[44−46] The protein molecules were treated as fixed with the binding site center defined at a carbonyl oxygen of Ser214 and the binding site radius of 15 Å. The distance constraints were set up to increase the preference of interaction between (a) inhibitor phosphorus atom and the hydroxide oxygen of protease Ser195 (distance range was defined between 2.2 and 4.0 Å), (b) the terminal carbon of Ala/nVal side chain of ligand P1 position and enzyme S1 binding pocket set at *γ*-carbon of Ile190 (distance range: 5.5−6.5 Å for Ala and 2.2−5.0 Å for nVal), (c) Asp *γ*-carbon of the inhibitor (P2 position) and PR3 *ε*-amine nitrogen of Lys99 (distance range 2.0−5.0 Å),and (d) ligand P3−P4 amide bond nitrogen and Val216 carbonyl oxygen of the receptor (distance range 2.0−5.0 Å). The lowest energy binding poses obtained from docking simulations were then employed in quantum chemical calculations of interaction energy between PR3 amino acid residues and Bt-Val4 fragment of inhibitor to explain the differences in activity of **11** toward human and macaque enzyme. *hum*PR3 or *mac*PR3 binding site was represented by all amino acid residues within 6 Å of inhibitor fragment considered herein. Because of the presence of disulfide bridge in the vicinity of inhibitor molecule, covalently linked Cys168 and Cys182 residues were included as a single monomer. Arg177 was found to be hydrogen-bonded to Asn98 and Asn180 residues. To avoid disrupting the hydrogen bonding network, these three residues were also considered as a monomer. The remaining 15 PR3 residues were included separately. The dangling bonds resulting from cutting the residues out of the protein scaffold were saturated with hydrogen atoms. PR3−inhibitor binding energy was calculated in a pairwise manner at the second-order Møller−Plesset level of theory (MP2) using 6-31+G(d) basis set[47−49] and counterpoise correction to eliminate basis set superposition error.[50] Quantum chemical calculations were performed in Gaussian09 program.[51]

ASSOCIATED CONTENT

Ⓢ Supporting Information

The Supporting Information is available free of charge on the ACS Publications website at DOI: 10.1021/acs.jmedchem.7b01416.

Spectroscopic data of synthesized inhibitors; supporting Information includes ^{1}H NMR spectra together with SMILES for compounds **1**−**11** (PDF)

Docking poses for **1**, **2**, **8**, and **11** with *hum*PR3 and **11** with *mac*R3 (ZIP)

Compound data (CSV)

AUTHOR INFORMATION

Corresponding Author
*Phone: (0033) 2 47 36 62 53. E-mail: brice.korkmaz@inserm.fr.

ORCID ⊙
Edyta Dyguda-Kazimierowicz: 0000-0002-9154-5107
Adam Lesner: 0000-0001-8335-3431
Brice Korkmaz: 0000-0002-5159-8706

Author Contributions
Carla Guarino and Natalia Gruba contributed equally to this work. Brice Korkmaz supervised the work. Brice Korkmaz and Adam Lesner participated in the research design. Carla Guarino, Natalia Gruba, Renata Grzywa, Edyta Dyguda-Kazimierowicz, Yveline Hamon, Monika Legowska, Marcin Skoreński, Sandrine Dallet-Choisy, Sylvain Marchand-Adam, and Christine Kellenberger conducted the experiments. Brice Korkmaz, Adam Lesner, Francis Gauthier, Marcin Sienczyk, and Dieter E. Jenne performed data analyses. Brice Korkmaz wrote the manuscript. All authors contributed to the writing and revision processes of the manuscript.

Notes
The authors declare no competing financial interest.

ABBREVIATIONS USED

ABP, activity-based probe; α1PI, alpha-1-proteinase inhibitor; ABZ, *ortho*-aminobenzoic acid; Bt, biotin; HPLC, high performance liquid chromatography; CG, cathepsin G; CF, cystic fibrosis; EDDnp, *N*-(2.4-dinitrophenyl)ethylenediamine; FRET, fluorescence resonance energy transfer; GPA, granulomatosis with polyangiitis; hum, human; NE, neutrophil elastase; NSP, neutrophil serine protease; PBS, phosphate-buffered saline; PEG, polyethlene glycol; PMN, polymorpho-nuclear neutrophil; pNA, *para*-nitroaniline; PR3, proteinase 3; WB, Western blot

REFERENCES

(1) Pham, C. T. Neutrophil serine proteases: specific regulators of inflammation. *Nat. Rev. Immunol.* **2006**, *6*, 541−550.

(2) Pham, C. T. Neutrophil serine proteases fine-tune the inflammatory response. *Int. J. Biochem. Cell Biol.* **2008**, *40*, 1317−1333.

(3) Perera, N. C.; Wiesmuller, K. H.; Larsen, M. T.; Schacher, B.; Eickholz, P.; Borregaard, N.; Jenne, D. E. NSP4 is stored in azurophil granules and released by activated neutrophils as active endoprotease with restricted specificity. *J. Immunol.* **2013**, *191*, 2700−2707.

(4) Owen, C. A. Roles for proteinases in the pathogenesis of chronic obstructive pulmonary disease. *Int. J. Chronic Obstruct. Pulm. Dis.* **2008**, *3*, 253−268.

(5) Korkmaz, B.; Horwitz, M.; Jenne, D. E.; Gauthier, F. Neutrophil elastase, proteinase 3 and cathepsin G as therapeutic targets in human diseases. *Pharmacol. Rev.* **2010**, *62*, 726−759.

(6) Korkmaz, B.; Lesner, A.; Guarino, C.; Wysocka, M.; Kellenberger, C.; Watier, H.; Specks, U.; Gauthier, F.; Jenne, D. E. Inhibitors and antibody fragments as potential anti-inflammatory therapeutics targeting neutrophil proteinase 3 in human disease. *Pharmacol. Rev.* **2016**, *68*, 603−630.

(7) Korkmaz, B.; Kellenberger, C.; Viaud-Massuard, M. C.; Gauthier, F. Selective inhibitors of human neutrophil proteinase 3. *Curr. Pharm. Des.* **2013**, *19*, 966−976.

(8) Jenne, D. E.; Tschopp, J.; Ludemann, J.; Utecht, B.; Gross, W. L. Wegener's autoantigen decoded. *Nature* **1990**, *346*, 520.

(9) Kallenberg, C. G. Pathogenesis of PR3-ANCA associated vasculitis. *J. Autoimmun.* **2008**, *30*, 29−36.

(10) Kallenberg, C. G.; Heeringa, P.; Stegeman, C. A. Mechanisms of Disease: pathogenesis and treatment of ANCA-associated vasculitides. *Nat. Clin. Pract. Rheumatol.* **2006**, *2*, 661−670.

(11) Loison, F.; Zhu, H.; Karatepe, K.; Kasorn, A.; Liu, P.; Ye, K.; Zhou, J.; Cao, S.; Gong, H.; Jenne, D. E.; Remold-O'Donnell, E.; Xu, Y.; Luo, H. R. Proteinase 3-dependent caspase-3 cleavage modulates neutrophil death and inflammation. *J. Clin. Invest.* **2014**, *124*, 4445−4458.

(12) Fujinaga, M.; Chernaia, M. M.; Halenbeck, R.; Koths, K.; James, M. N. The crystal structure of PR3, a neutrophil serine proteinase antigen of wegener's granulomatosis antibodies. *J. Mol. Biol.* **1996**, *261*, 267−278.

(13) Korkmaz, B.; Moreau, T.; Gauthier, F. Neutrophil elastase, proteinase 3 and cathepsin G: physicochemical properties, activity and physiopathological functions. *Biochimie* **2008**, *90*, 227−242.

(14) Hedstrom, L. Serine protease mechanism and specificity. *Chem. Rev.* **2002**, *102*, 4501−4523.

(15) Korkmaz, B.; Hajjar, E.; Kalupov, T.; Reuter, N.; Brillard-Bourdet, M.; Moreau, T.; Juliano, L.; Gauthier, F. Influence of charge distribution at the active site surface on the substrate specificity of human neutrophil protease 3 and elastase. A kinetic and molecular modeling analysis. *J. Biol. Chem.* **2007**, *282*, 1989−1897.

(16) Bode, W.; Meyer, E., Jr.; Powers, J. C. Human leukocyte and porcine pancreatic elastase: x-ray crystal structures, mechanism, substrate specificity, and mechanism-based inhibitors. *Biochemistry* **1989**, *28*, 1951−1963.

(17) Bode, W.; Wei, A. Z.; Huber, R.; Meyer, E.; Travis, J.; Neumann, S. X-ray crystal structure of the complex of human leukocyte elastase (PMN elastase) and the third domain of the turkey ovomucoid inhibitor. *EMBO. J.* **1986**, *5*, 2453−2458.

(18) Guarino, C.; Legowska, M.; Epinette, C.; Kellenberger, C.; Dallet-Choisy, S.; Sienczyk, M.; Gabant, G.; Cadene, M.; Zoidakis, J.; Vlahou, A.; Wysocka, M.; Marchand-Adam, S.; Jenne, D. E.; Lesner, A.; Gauthier, F.; Korkmaz, B. New selective peptidyl di(chlorophenyl) phosphonate esters for visualizing and blocking neutrophil proteinase 3 in human diseases. *J. Biol. Chem.* **2014**, *289*, 31777−31791.

(19) Oleksyszyn, J.; Powers, J. C. Irreversible inhibition of serine proteases by peptide derivatives of (alpha-aminoalkyl)phosphonate diphenyl esters. *Biochemistry* **1991**, *30*, 485−493.

(20) Powers, J. C.; Asgian, J. L.; Ekici, O. D.; James, K. E. Irreversible inhibitors of serine, cysteine, and threonine proteases. *Chem. Rev.* **2002**, *102*, 4639−4750.

(21) Mucha, A.; Kafarski, P.; Berlicki, L. Remarkable potential of the alpha-aminophosphonate/phosphinate structural motif in medicinal chemistry. *J. Med. Chem.* **2011**, *54*, 5955−5980.

(22) Sienczyk, M.; Oleksyszyn, J. Irreversible inhibition of serine proteases - design and in vivo activity of diaryl alpha-amino-phosphonate derivatives. *Curr. Med. Chem.* **2009**, *16*, 1673−1687.

(23) Grzywa, R.; Sienczyk, M. Phosphonic esters and their application of protease control. *Curr. Pharm. Des.* **2013**, *19*, 1154−1178.

(24) Kasperkiewicz, P.; Poreba, M.; Snipas, S. J.; Parker, H.; Winterbourn, C. C.; Salvesen, G. S.; Drag, M. Design of ultrasensitive probes for human neutrophil elastase through hybrid combinatorial substrate library profiling. *Proc. Natl. Acad. Sci. U. S. A.* **2014**, *111*, 2518−2523.

(25) Kam, C. M.; Kerrigan, J. E.; Dolman, K. M.; Goldschmeding, R.; Von dem Borne, A. E.; Powers, J. C. Substrate and inhibitor studies on proteinase 3. *FEBS Lett.* **1992**, *297*, 119−123.

(26) Grzywa, R.; Burchacka, E.; Lecka, M.; Winiarski, L.; Walczak, M.; Lupicka-Slowik, A.; Wysocka, M.; Burster, T.; Bobrek, K.; Csencsits-Smith, K.; Lesner, A.; Sienczyk, M. Synthesis of Novel phosphonic-type activity-based probes for neutrophil serine proteases and their application in spleen lysates of different organisms. *ChemBioChem* **2014**, *15*, 2605−2612.

(27) Korkmaz, B.; Jenne, D. E.; Gauthier, F. Relevance of the mouse model as a therapeutic approach for neutrophil proteinase 3-associated human diseases. *Int. Immunopharmacol.* **2013**, *17*, 1198−1205.

(28) Grzywa, R.; Dyguda-Kazimierowicz, E.; Sienczyk, M.; Feliks, M.; Sokalski, W. A.; Oleksyszyn, J. The molecular basis of urokinase inhibition: from the nonempirical analysis of intermolecular interactions to the prediction of binding affinity. *J. Mol. Model.* **2007**, *13*, 677−683.

(29) Korkmaz, B.; Poutrain, P.; Hazouard, E.; de Monte, M.; Attucci, S.; Gauthier, F. L. Competition between elastase and related proteases from human neutrophil for binding to alpha1-protease inhibitor. *Am. J. Respir. Cell Mol. Biol.* **2005**, *32*, 553−559.

(30) Kasperkiewicz, P.; Altman, Y.; D'Angelo, M.; Salvesen, G. S.; Drag, M. Toolbox of fluorescent probes for parallel imaging reveals uneven location of serine proteases in neutrophils. *J. Am. Chem. Soc.* **2017**, *139*, 10115−10125.

(31) Epinette, C.; Croix, C.; Jaquillard, L.; Marchand-Adam, S.; Kellenberger, C.; Lalmanach, G.; Cadene, M.; Viaud-Massuard, M. C.; Gauthier, F.; Korkmaz, B. A selective reversible azapeptide inhibitor of human neutrophil proteinase 3 derived from a high affinity FRET substrate. *Biochem. Pharmacol.* **2012**, *83*, 788−796.

(32) Lechtenberg, B. C.; Kasperkiewicz, P.; Robinson, H.; Drag, M.; Riedl, S. J. The elastase-PK101 structure: mechanism of an ultrasensitive activity-based probe revealed. *ACS Chem. Biol.* **2015**, *10*, 945−951.

(33) Kalupov, T.; Brillard-Bourdet, M.; Dade, S.; Serrano, H.; Wartelle, J.; Guyot, N.; Juliano, L.; Moreau, T.; Belaaouaj, A.; Gauthier, F. Structural characterization of mouse neutrophil serine proteases and identification of their substrate specificities: relevance to mouse models of human inflammatory diseases. *J. Biol. Chem.* **2009**, *284*, 34084−34091.

(34) Guarino, C.; Hamon, Y.; Croix, C.; Lamort, A. S.; Dallet-Choisy, S.; Marchand-Adam, S.; Lesner, A.; Baranek, T.; Viaud-Massuard, M. C.; Lauritzen, C.; Pedersen, J.; Heuze-Vourc'h, N.; Si-Tahar, M.; Firatli, E.; Jenne, D. E.; Gauthier, F.; Horwitz, M. S.; Borregaard, N.; Korkmaz, B. Prolonged pharmacological inhibition of cathepsin C results in elimination of neutrophil serine proteases. *Biochem. Pharmacol.* **2017**, *131*, 52−67.

(35) Jegot, G.; Derache, C.; Castella, S.; Lahouassa, H.; Pitois, E.; Jourdan, M. L.; Remold-O'Donnell, E.; Kellenberger, C.; Gauthier, F.; Korkmaz, B. A substrate-based approach to convert serpinB1 into a specific inhibitor of proteinase 3, the Wegener's granulomatosis autoantigen. *FASEB J.* **2011**, *25*, 3019−3031.

(36) Sienczyk, M.; Oleksyszyn, J. Inhibition of trypsin and urokinase by cbz-amino(4-guanidinophenyl)methanephosphonate aromatic ester derivatives: the influence of the ester group on their biological activity. *Bioorg. Med. Chem. Lett.* **2006**, *16*, 2886−2890.

(37) Oleksyszyn, J.; Powers, J. C. Irreversible inhibition of serine proteases by peptidyl derivatives of alpha-aminoalkylphosphonate diphenyl esters. *Biochem. Biophys. Res. Commun.* **1989**, *161*, 143−149.

(38) Korkmaz, B.; Attucci, S.; Hazouard, E.; Ferrandiere, M.; Jourdan, M. L.; Brillard-Bourdet, M.; Juliano, L.; Gauthier, F. Discriminating between the activities of human neutrophil elastase and proteinase 3 using serpin-derived fluorogenic substrates. *J. Biol. Chem.* **2002**, *277*, 39074−39081.

(39) Tian, W. X.; Tsou, C. L. Determination of the rate constant of enzyme modification by measuring the substrate reaction in the presence of the modifier. *Biochemistry* **1982**, *21*, 1028−1032.

(40) Singh, J.; Petter, R. C.; Baillie, T. A.; Whitty, A. The resurgence of covalent drugs. *Nat. Rev. Drug Discovery* **2011**, *10*, 307−317.

(41) Biasini, M.; Bienert, S.; Waterhouse, A.; Arnold, K.; Studer, G.; Schmidt, T.; Kiefer, F.; Cassarino, T. G.; Bertoni, M.; Bordoli, L.; Schwede, T. SWISS-MODEL: modelling protein tertiary and quaternary structure using evolutionary information. *Nucleic Acids Res.* **2014**, *42*, W252−W258.

(42) Burkert, U.; Allinger, N. L. *Molecular Mechanics*; ACS Monograph 177; American Chemical Society: Washington, DC, 1982.

(43) ten Brink, T.; Exner, T. E. pK(a) based protonation states and microspecies for protein-ligand docking. *J. Comput.-Aided Mol. Des.* **2010**, *24*, 935−942.

(44) Korb, O.; Stutzle, T.; Exner, T. E. Empirical scoring functions for advanced protein-ligand docking with plants. *J. Chem. Inf. Model.* **2009**, *49*, 84−96.

(45) Korb, O.; Stützle, T.; Exner, T. E. PLANTS: application of ant colony optimization to structure-based drug design. *Lecture. Notes. in. Comput. Sci.* **2006**, *4150*, 247−258.

(46) Korb, O.; Stützle, T.; Exner, T. E. An ant colony optimization approach to flexible protein-ligand docking. *Swarm. Intell.* **2007**, *1*, 115−134.

(47) Hariharan, P. C.; Pople, J. A. The influence of polarization functions on molecular-orbital hydrogenation energies. *Theoret. Chimica. Acta.* **1973**, *28*, 213−222.

(48) Francl, M. M.; Pietro, W. J.; Hehre, W. J.; Binkley, J. S.; DeFrees, D. J.; Pople, J. A.; Gordon, M. S. Self-consistent molecular orbital methods. XXIII. A polarization-type basis set for second-row elements. *J. Chem. Phys.* **1982**, *77*, 3654−3665.

(49) Krishnan, R.; Binkley, J. S.; Seeger, R.; Pople, J. A. Self-consistent molecular orbital methods. XX. A basis set for correlated wave functions. *J. Chem. Phys.* **1980**, *72*, 650−654.

(50) Boys, S.; Bernardi, F. The calculation of small molecular interactions by the differences of separate total energies. some procedures with reduced errors. *Mol. Phys.* **1970**, *19*, 553−566.

(51) Frisch, M. J.; Trucks, G. W.; Schlegel, H. B.; Scuseria, G. E.; Robb, M. A.; Cheeseman, J. R.; Scalmani, G.; Barone, V.; Petersson, G. A.; Nakatsuji, H.; Li, X.; Caricato, M.; Marenich, A.; Bloino, J.; Janesko, B. G.; Gomperts, R.; Mennucci, B.; Hratchian, H. P.; Ortiz, J. V.; Izmaylov, A. F.; Sonnenberg, J. L.; Williams-Young, D.; Ding, F.; Lipparini, F.; Egidi, F.; Goings, J.; Peng, B.; Petrone, A.; Henderson, T.; Ranasinghe, D.; Zakrzewski, V. G.; Gao, J.; Rega, N.; Zheng, G.; Liang, W.; Hada, M.; Ehara, M.; Toyota, K.; Fukuda, R.; Hasegawa, J.; Ishida, M.; Nakajima, T.; Honda, Y.; Kitao, O.; Nakai, H.; Vreven, T.; Throssell, K.; Montgomery, Jr., J. A.; Peralta, J. E.; Ogliaro, F.; Bearpark, M.; Heyd, J. J.; Brothers, E.; Kudin, K. N.; Staroverov, V. N.; Keith, T.; Kobayashi, R.; Normand, J.; Raghavachari, K.; Rendell, A.; Burant, J. C.; Iyengar, S. S.; Tomasi, J.; Cossi, M.; Millam, J. M.; Klene, M.; Adamo, C.; Cammi, R.; Ochterski, J. W.; Martin, R. L.; Morokuma, K.; Farkas, O.; Foresman, J. B.; Fox, D. J. *Gaussian 09*, revision E.01; Gaussian Inc: Wallingford, CT, 2009.

(52) Korkmaz, B.; Attucci, S.; Juliano, M. A.; Kalupov, T.; Jourdan, M. L.; Juliano, L.; Gauthier, F. Measuring elastase, proteinase 3 and cathepsin G. *Nat. Protoc.* **2008**, *3*, 991−1000.